Earth Surf. Dynam. Discuss., 1, 141–175, 2013
www.earth-surf-dynam-discuss.net/1/141/2013/
doi:10.5194/esurfd-1-141-2013

Earth Surface Dynamics Discussions
Open Access

A two-sided approach to estimate heat transfer processes within the active layer of rock glacier Murtèl-Corvatsch

M. Scherler, S. Schneider, M. Hoelzle, and C. Hauck

Departement of Geosciences, University of Fribourg, Chemin du Musée 4, 1700 Fribourg, Switzerland

Received: 7 June 2013 – Accepted: 20 June 2013 – Published: 2 July 2013

Correspondence to: M. Scherler (martin.scherler@unifr.ch)

Published by Copernicus Publications on behalf of the European Geosciences Union.

Abstract

The thermal regime of permafrost in scree slopes and rock glaciers is characterized by the importance of air flow driven convective and advective heat transfer processes. These processes are supposed to be part of the energy balance in the active layer of rock glaciers leading to lower subsurface temperatures than would be expected at the lower limit of discontinues high mountain permafrost. In this study, new parameterizations were introduced in a numerical soil model to simulate permafrost temperatures observed in a borehole at rock glacier Murtèl in the Swiss Alps in the period from 1997 to 2008. A soil heat sink and source layer was implemented within the active layer which was parameterized experimentally to account for and quantify the contribution of air flow driven heat transfer on the measured permafrost temperatures. The experimental model calibration process yielded a value of about 28.9 Wm^{-2} for the heat sink during the period from mid September to mid January and one of 26 Wm^{-2} for the heat source in the period from June to mid September. Energy balance measurements, integrated over a 3.5 m thick blocky surface layer, showed seasonal deviations between a zero energy balance and the calculated sum of the energy balance components of around 6.8 Wm^{-2} in fall/winter, -2.2 Wm^{-2} in winter/spring and around -5.6 Wm^{-2} in summer. The calculations integrate heat exchange processes including thermal radiation between adjacent blocks, turbulent heat flux and energy storage change in the blocky surface layer. Finally, it is hypothesized that these deviations approximately equal unmeasured freezing and thawing processes within the blocky surface layer.

1 Introduction

Permafrost in high mountain environments is a common phenomenon at altitudes above 2400 m a.s.l. It can be found in areas with various subsurface characteristics such as solid rock, weathered rock with a fine grained surface cover, or talus slopes consisting of coarse debris. At debris covered sites in high mountains relatively cold

ESurfD

1, 141–175, 2013

permafrost can be found at lower altitudes than would be expected form prevailing mean annual air temperatures. One explanation for this are the thermal properties of blocky surfaces, which may lead to the existence of permafrost at sites, where without such ground characteristics permafrost would not develop (e.g. Harris and Pedersen, 1998; Delaloye and Lambiel, 2005; Hanson and Hoelzle, 2004). One special permafrost form in talus slopes are rock glaciers. This type of permafrost is characterized by ice-supersaturated sediments covered by large blocks (Arenson et al., 2002). Rock glaciers often show lobes of tens of meters wavelengths and a few meters in amplitude at the surface (Kääb et al., 1998). Besides the subsurface material, the ice and water content of the ground, the energy balance at the surface is the most important factor for the existence of permafrost. Due to the coarse surface layer of a rock glacier with boulders of up to 10 m in diameter the determination of an energy balance at the surface is a complex problem. The surface in this case is rather to be seen as a blocky surface layer of several meters in thickness comprising a large part of the blocky surface layer with voids and the air column above (Herz et al., 2003). In surface energy balance measurements even under less complicated circumstances, e.g. arctic plains with sparse vegetation, there are usually deviation terms of up to 20 Wm^{-2} to a zero energy balance reported due to method related errors and parameterizations (Westermann et al., 2009). A study by Mittaz et al. (2000) at rock glacier Murtèl found deviations to a zero energy balance of up to 78 Wm^{-2} in winter and -130 Wm^{-2} in summer, which were explained by advective heat transfer processes through voids within the debris.

Several processes of advective and convective air circulation in blocky material have been described in literature: A convective process is the Balch effect (Balch, 1900) which describes the replacement of warm air with cold air within the voids of the blocky material due to density differences. An additional convective/advective process on inclined blocky slopes called the chimney effect was first described in a study from Wakonigg (1996). In winter relatively warm air within the blocky layer ascends beneath the snow cover creating melting holes in the upper part of the slope which facilitates

ESurfD
1, 141–175, 2013

the aspiration of cold air inside the talus slope (Delaloye et al., 2003). Discharge of cold air in summer driven by gravity may lead to advective heat transfer by air circulation (Delaloye et al., 2003). Further studies stressing the importance of air circulation within the active layer of coarse blocky scree slopes for the Alps have been presented by e.g. Vonder Mühll et al. (2003). Tanaka et al. (2000) describe these effects in a modeling study for mountaineous regions in Korea and Japan. Similar effects are also described for antropogenic structures, i.e. crushed rock highway embankment (e.g. Binxiang et al., 2007). Harris and Pedersen (1998) suggested an advective process which is characterized by continuous air exchange between the voids and the atmosphere. Air exchange with the atmosphere will result in almost instantaneous warming and cooling of the blocky debris to a considerable depth in response to changes in air temperature. Heat transfer by water flow from precipitation between the blocks is expected to lead to a reduction of the temperature gradients and in the blocky surface layer, which will be reflected in the thermal conduction term and the storage change (integrated over the entire surface layer).

In model studies aiming on the simulation of the hydrothermal regime and the response of permafrost to climate change, three-dimensional energy exchange processes in the active layer are often approximated by very low effective thermal conductivities of the coarse blocky material, i.e. the surface layer is treated as a "thermal semi-conductor" (see e.g. Cheng et al., 2007 or Gruber and Hoelzle, 2008).

The aim of this study was to compare the energy balance of a calibrated one-dimensional heat and mass transfer model, which was used in an earlier study to simulate the thermal regime of the rock glacier Murtèl under the influence of climate change scenarios (see Scherler et al., 2013), to a measured energy balance. Here, a more process oriented approach than a thermal semi-conductive layer is presented to calibrate the one-dimensional model for the complex three-dimensional processes within the active layer of rock glacier Murtèl-Corvatsch. A seasonally variable heat source and sink layer has been implemented in the active layer to simulate the three-dimensional energy transfer processes. This approach allowed for the indirect quantification of the total

ESurfD
1, 141–175, 2013

energy exchange by three-dimensional heat transfer processes. In the measured energy balance the use of additional terms for radiative heat transfer between the blocks (see e.g. Kunii and Smith, 1960; Fillion et al., 2011), heat storage change and turbulent heat flux in the blocky surface layer allowed to approximate seasonal freezing and thawing processes within the active layer and the permafrost.

2 Site description

The site of this study is rock glacier Murtèl-Corvatsch in the Upper Engadine, Switzerland. The rock glacier reaches from 2850 to 2620 m a.s.l. and is 400 m long and 200 m wide, facing north-northwest. At the site a 60 m deep borehole was drilled and equipped with thermistors in 1987 which have been manually logged in 1 month intervals until 1992 and since than data is stored automatically by a logger collecting temperature data in 6 h intervals (Hoelzle et al., 2002). A micrometeorological station established in 1997 at 2700 m a.s.l. next to the borehole measures shortwave and long-wave incoming and outgoing radiation, air temperature, surface temperature, relative humidity, wind speed and direction (Mittaz et al., 2000; Hoelzle and Gruber, 2008). The site is characterized by a coarse blocky surface layer of approximately 3–3.5 m in thickness above a massive ice core down to 28 m and frozen blocky layer underneath, reaching from 28 to 50 m probably adjacent to the bedrock (Arenson et al., 2002). The ice core has a temperature of −2 °C at 10 m depth and −1.4 °C at 25 m depth. The active layer has a thickness of 3.2 m on average. The diameters of the boulders forming the surface layer are in the range of decimetres up to several meters. The coparison of the stratigraphy of the studied borehole with the stratigraphies of two boreholes located within a distance of 30 m shows significant small scale heterogeneities in the rock glacier (Vonder Mühll et al., 2001; Arenson et al., 2010). In direct proximity of the rock glacier, areas with fine grained subsurface material/soil as well as solid rock exist which show no permafrost conditions (Schneider et al., 2012). The rocks at the site mainly consist of metamorphic granodiorite and basalt (Schneider et al., 2012). Annual precipitation at

ESurfD
1, 141–175, 2013

the site is about 900 mm (982 mm St Moritz 1951–1980; 856 mm Piz Corvatsch 1984–1997). Typical maximum snow cover thickness is between 1 m and 2 m. Mean annual air temperature is −1.7 °C for the observation period of March 1997 to March 2008. The study site has been described in more detail by Haeberli et al. (1988); Hoelzle et al. (2002); Vonder Mühll et al. (2003); Schneider et al. (2012).

2.1 Methods

2.2 Meteorological measurements

The meteorological parameters air temperature, surface temperature, relative humidity, incoming and outgoing shortwave and longwave radiation, wind speed and snow height, are measured by a micrometeorological station directly at the study site (Mittaz et al., 2000; Hoelzle and Gruber, 2008). Data for this study have been measured at the station for the period from January 1997 to March 2008 in a 10 min interval and were stored as 30 min averages by the logger (see Table 1). Precipitation data is taken from a nearby station of MeteoSwiss, located at the summit of Piz Corvatsch. Data gaps in the on-site measurements, which are caused by lightning, avalanches, or hoarfrost were reconstructed with measurements from the summit station, corrected by the use of correlation coefficients determined between the two stations. This completed meteorological data set consisting of incoming shortwave and longwave radiation, air temperature, wind speed, relative humidity, and precipitation is used as input in the Coup Model (see Sect. 2.4). For the energy balance calculations the original data is left incomplete.

2.3 Energy balance

Generally, the energy balance at seasonally snow covered sites is refering to a unit area and includes the components net short-wave and long-wave radiation, turbulent fluxes composed of sensible heat and latent heat, ground heat flux, melt energy of

ESurfD
1, 141–175, 2013

the snow, and heat flux through the snow cover. The corresponding energy balance (Williams and Smith, 1989) at such a site is given as:

$$Q_r + Q_h + Q_{le} + Q_g + Q_m + Q_s = 0 \quad (1)$$

where Q_r is the net radiation, Q_h is the sensible heat flux, Q_{le} is the latent heat flux, Q_g is the ground heat flux, Q_m is the melt energy at the snow surface, and Q_s is the heat flux through the snow cover. Following the convention (Oke, 1988) heat fluxes towards the surface are denoted positive and heat fluxes away from the surface are denoted negative (see Fig. 1).

Due to the blocky surface layer at rock glacier Murtèl-Corvatsch, in this study the energy balance within a volumetric blocky surface layer was studied. This contrasts to the approach of other energy balance studies, which refer to the energy balance of a two-dimensional unit area (see e.g. Stocker-Mittaz, 2002; Westermann et al., 2009). Processes within the blocky layer, added to the purely conductive ground heat flux usually applied, are: convective or advective heat transfer by air flow in the voids between the blocks, net longwave radiation between adjacent blocks, melt and freezing energy within the active layer and at the permafrost table, and the heat storage change. The formulation of the energy balance term Q_g of Eq. (1) then becomes:

$$Q_g = Q_{g_{al}} + Q_{g_{pf}} + Q_{le_{al}} + Q_{h_{al}} + Q_{r_{al}} + \Delta Q_{storage} + Q_{m_{al}} + Q_{m_{pf}} \quad (2)$$

where $Q_{g_{al}}$ is the conductive heat flux through the blocks of the active layer, $Q_{g_{pf}}$ is the ground heat flux through the permafrost table, $Q_{le_{al}}$ and $Q_{h_{al}}$ are the latent heat flux and the sensible heat flux in the voids between the blocks, $Q_{r_{al}}$ is the net radiative heat flux between the blocks, $\Delta Q_{storage}$ is a source or sink term for heat energy in the blocks, $Q_{m_{al}}$ and $Q_{m_{pf}}$ is the melt/freezing energy used in the active layer and at the permafrost table.

ESurfD
1, 141–175, 2013

Energy balance components were calculated on an hourly time step (except melt energy, for which 24 h intervals are used) and were then averaged to monthly and seasonal values (June–September; October–January; February–May) as shown in Fig. 2. In the following the individual terms of Eqs. (1) and (2) are explained in detail.

2.3.1 Radiative heat flux

Q_{rad} is the net radiation at the surface and is calculated from direct radiation measurments at the micrometeorological station. The radiation measurements comprise incoming and outgoing short-wave and long-wave radiation, see Eq. (3):

$$Q_{\mathrm{rad}} = L_{\downarrow} + S_{\downarrow} - L_{\uparrow} - S_{\uparrow} \tag{3}$$

where L denotes longwave radiation and S denotes shortwave radiation.

The slope angle at the site was approximated by 10°, which reduces the radiation density on the surface. A further reduction of radiation density is expected due to surface roughness and shadow effects caused by the shape of the blocks. Therfore a geometrical factor was included, which was approximated by an additional slope angle of 5°.

2.3.2 Turbulent fluxes

The turbulent heat fluxes within the blocks and at the surface blocky layer are calculated following Oke (1988). The sensible heat flux, Q_{h}, from the surface to the air is:

$$Q_{\mathrm{h}} = -C_{\mathrm{a}}\kappa^2 z^2 \left(\frac{\Delta\overline{u}}{\Delta z}\frac{\Delta\overline{T}}{\Delta z}\right)(\Phi_{\mathrm{M}}\Phi_{\mathrm{H}})^{-1} \tag{4}$$

where C_{a} is the heat capacity of air, κ is the von Karman constant, $\Delta\overline{u}$ is the wind speed gradient between sensor and ground surface, Δz is the height, $\Delta\overline{T}$ is the temperature gradient between sensor and ground surface, z is the surface roughness, Φ_{H} is a

ESurfD
1, 141–175, 2013

dimensionless stability function for heat and Φ_M is a dimensionless stability function to account for curvature of the logarithmic wind profile due to buoyancy effects.

The latent heat flux at the ground surface is given by:

$$Q_{le} = -L_v \kappa^2 z^2 \left(\frac{\Delta \overline{u}}{\Delta z} \frac{\Delta \overline{\rho_v}}{\Delta z} \right) (\Phi_M \Phi_V)^{-1} \quad (5)$$

where L_v is the latent heat of evaporation, $\Delta \overline{\rho_v}$ is the gradient in specific humidity between the ground surface and the humidity sensor at 2 m height, and Φ_V is a dimensionless stability function for vapour.

The stability functions in Eqs. (4) and (5) are calculated as:

in the stable case (R_i positive)

$$(\Phi_M \Phi_x)^{-1} = (1 - 5R_i)^2 \quad (6)$$

in the unstable case (R_i negative)

$$(\Phi_M \Phi_x)^{-1} = (1 - 16R_i)^{3/4} \quad (7)$$

where Φ_x is the respective stability function (Φ_H or Φ_V), R_i is the Richardson number to categorize atmospheric stability and the state of turbulence in the lower atmosphere calculated as:

$$R_i = \frac{g}{\overline{T}} \frac{(\Delta \overline{T} / \Delta z)}{(\Delta \overline{u} / \Delta z)^2} \quad (8)$$

where g is acceleration due to gravity and $\overline{T}$ is the mean temperature in the layer Δz.

2.3.3 Melt energy

The melt energy at the surface of the snow cover is calculated according to the difference in snow height in 24 h intervals, as measured by an ultrasonic sensor at the

ESurfD
1, 141–175, 2013

micrometeorological station (see Table 1). Snow melt is assumed to occur at air temperatures above −3 °C and values of more than 0.2 m snow height difference within a 24 h period is considered as a measurement error and thus not taken into account. Snow density is assumed to be constant at 300 kg m^{-3}. The melt energy is thus given as:

$$Q_{\mathrm{m}} = \Delta h \rho_{\mathrm{s}} L_f \tag{9}$$

where Δh is the difference in snow height, ρ_{s} is the density of snow, and L_f is the latent heat of thawing.

2.3.4 Ground heat flux

The ground heat flux is calculated based on borehole temperature measurements at 0.55 m, 1.55 m, 2.55 m and 3.55 m depth assuming a thermal conductivity k_r of 2.5 Wm^{-2} in the Fourier heat conduction equation (see Eq. 10) which is considered to be appropriate for the solid metamorphic rocks found within the blocky layer. The values were then multiplied by a correction factor 1/3 to account for the reduction of conductive heat fluxes within the air filled voids between the blocks. In contrast to the Coup Model simulations (see Sect. 2.4), changes in thermal conductivity due to water and ice content as well as latent heat processes are not accounted for here.

$$Q_{\mathrm{g}} = \frac{k_r}{3} \sum_{i=1}^{3} \frac{\Delta T_i}{\Delta z_i} \tag{10}$$

where Δz_i are the respective layer thicknesses (here, 1 m). The heat flux within the permafrost layer, $Q_{\mathrm{g_{pf}}}$, is calculated likewise using the thermal conductivity of ice and temperatures measured at 3.55 m and 4.55 m depth during the winter period (October–January) and with a 3.55 m temperature fixed at 0 °C during the spring and summer period (February–September).

ESurfD
1, 141–175, 2013

2.3.5 Net-radiation between adjacent blocks

Due to the studied volumetric layer, a term accounting for radiative processes between the blocks due to temperature differences has been included in the energy balance (Eq. 2) (Kunii and Smith, 1960). The temperature gradient from the surface to the permafrost table leads to immediate heat flow from the warmer upper blocks to colder lower blocks in the active layer. This process is based on the emission and the absorption of thermal/longwave radiation between adjacent blocks of different temperature. Both blocks will emit longwave radiation (black body/gray body radiation) following the Stefan-Boltzmann law:

$$P = \varepsilon \sigma A T^4 \tag{11}$$

where P is the emitted longwave radiation, ε is the emmisivity of the block (0.96) as determined by surface temperature and longwave radiation measurements, A is the area (here 1 m^2), T is the absolute temperature, and σ is the Stefan-Boltzmann constant.

In the case of two opposite blocks with an emissivity of $\varepsilon < 1$, the reflection of radiation has to be considered following McAdams (1954):

$$\varepsilon_{1,2} = \frac{1}{\frac{1}{\varepsilon_1} + \frac{1}{\varepsilon_2} - 1} = \frac{\varepsilon_1 \varepsilon_2}{\varepsilon_1 + \varepsilon_2 - \varepsilon_1 \varepsilon_2} \tag{12}$$

In the case where ε_1 equals ε_2, which is assumed for the blocks of the rock glacier, Eq. (12) becomes:

$$\varepsilon_{\text{eff}} = \frac{\varepsilon^2}{2\varepsilon - \varepsilon^2} \tag{13}$$

The calculation is based on the borehole temperatures at 0.55 m, 1.55 m, 2.55 m, and 3.55 m. Errors might arise from too high gradients due to measurement depth intervals of 1 m. Voids between individual blocks are assumed not to be larger than 0.33 m on average. Thus, the sum of the individual Q_r between thermistors has been approximated by a reduction to one third of the calculated values.

ESurfD
1, 141–175, 2013

2.3.6 Snow heat flux

The snow heat flux is the heat flux within the snow layer. It is calculated following the Fourier heat conduction equation:

$$Q_s = k_s \frac{T_s - T_{0.55}}{0.55 + h_s} \quad (14)$$

where T_s is the snow surface temperature, $T_{0.55}$ is the temperature of the sensor in 0.55 m depth, h_s is the snow height and the thermal conductivity of snow k_s is calculated following Devaux (1933) (see also Keller, 1994; Stocker-Mittaz, 2002):

$$k_s = 2.93 \left(\frac{\rho_{prec}^2}{1\,000\,000} + 0.1 \right) \quad (15)$$

where ρ_{prec} is the density of snow.

2.3.7 Energy storage

When looking at the energy balance of a volumetric layer the storage of energy has to be accounted for. The heating of blocks during the summer period will produce an energy sink term in the energy balance equation. The release of heat due to cooling of the blocks acts as an energy source in the balance equation (see Eq. 2). The storage change term is calculated as:

$$\Delta Q_{storage} = c_r \Delta T m_r \quad (16)$$

where c_r is the specific heat capacity of rock, ΔT is the daily temperature difference and m_r is the rock mass. The porosity of the blocky layer is assumed to be 40 %.

ESurfD
1, 141–175, 2013

2.4 Coup model

The model used in this study is a one-dimensional heat and mass transfer model for the soil-snow-atmosphere system (Coup Model; Jansson and Karlberg, 2011). The model was chosen for a sensitivity study involving transient hydrothermal simulations using RCM derived climate scenarios of the 21st century (see Scherler et al., 2013). The empirical parameterization used in the calibration of the model, as described below, was a part of this project. In this study, a detailed comparison of the simulated and the measured energy balance is presented.

Two coupled partial differential equations for water and heat flow are the core of the Coup Model. These equations are solved with an explicit forward difference method. A detailed description of the model including all its equations and parameters is given in Jansson and Karlberg (2011). Applications of the model are detailed in a number of studies (e.g. Johnsson and Lundin, 1991; Stähli et al., 1996; Bayard et al., 2005; Scherler et al., 2010, 2013). Processes which are important for permafrost such as freezing and thawing of the soil (Lundin, 1990) as well as the accumulation, metamorphosis, and melt of a snow cover (Gustafsson et al., 2001), are included in the model. The model is driven by air temperature, relative humidity, wind speed, global radiation, incoming longwave radiation and precipitation. The upper boundary condition is given by a surface energy balance at the soil-snow-atmosphere boundary layer. The lower boundary condition at the bottom of the soil column in a depth of 70 m is given as a zero heat flux and a seepage flow of percolating water. The model is initialized with an ice content of 85 % in the permafrost in depths of 3.4 to 22.4 m below the surface and a starting temperature of −1.5 °C.

To account for three-dimensional heat transfer by longwave radiation and air circulation between the blocks, which cannot be simulated directly in a one dimensional model, but are supposed to have a significant impact on the thermal regime of the active layer in coarse debris covered permafrost (Delaloye and Lambiel, 2005; Mittaz et al., 2000; Hanson and Hoelzle, 2004), a layer which serves as a heat source/sink

ESurfD
1, 141–175, 2013

is introduced in the model. It adds energy to the soil system in the summer season (June–mid September) and extracts energy in winter (mid September–mid January). This energy source/sink layer is parameterized based partly on knowledge taken from an observational study done by Mittaz et al. (2000), who found significant deviations to a zero energy balance in summer and winter in measurements at the Murtèl rock glacier site. The values for the parameterization were then adjusted experimentally during the calibration phase of the model. Heat source and heat sink are treated as constant in the respective seasons due to simplicity. Parameterization is considered as successful when measured borehole temperatures and simulated temperatures at two depths within the permafrost show the best fit. To reach near thermodynamic equilibrium conditions the model was run for four 11 yr cycles in the case with heat source and sink parameterization and for eleven 11 yr cycles in the case without heat pump. This discrepancy is due to the 85 % ice content in the respective layers (5.5 m and 10.5 m) which has to be melted in the case of no additional heat sink/source in the model before reaching an approximate thermodynamic equilibrium.

Results

2.5 Energy balance

Figure 2 and Tables 2, 3, and 4 show the seasonal energy balances at the study site from 1997 to 2007. Figure 2a is showing the measured energy balance components, Fig. 2b is showing the modeled energy balance components. In the measured energy balance, the following criteria were used to select seasons to be excluded in the energy balance calculations: (1) seasons with too many missing values overall (> 30 %), seasons missing important variables (i.e. surface temperature T_{ir} or long- and shortwave radiation), and (3) complete years with two missing seasons following the above criteria. The long term seasonal average energy balance is shown in Fig. 3. Measured and simulated energy balances differ significantly in most of the terms. Radiative heat flux at the surface is smaller in the model than in the measurements in the summer and

ESurfD
1, 141–175, 2013

winter season, whereas sensible heat flux is larger in the respective seasons. Latent heat is larger by a factor of two in the measurements compared to the simulation. In the model latent heat is always negative, i.e. flowing away from the surface. Melt energy is larger in the model during summer and equal from February to May. Overall heat fluxes are significantly higher in the measurements during the winter season.

Both measured and simulated energy balances have deviation terms to close the energy balance to zero. The deviations may arise from various sources which can differ between model and measurements, see also corresponding Sect. 3.1.9 in the Discussion.

Seasonal deviation terms of the measurements (only complete measurement years considered) range from 16.9 Wm^{-2} in October–February (Table 3 to $-13.3\,Wm^{-2}$ in February–May (Table 4). Deviation terms in the model range from 31.9 Wm^{-2} in June–September to $-1.0\,Wm^{-2}$ in February–May (see Fig. 2). The sum of the average seasonal deviations of the measurements (see Tables 2, 3, and 4) is equal to a net-melt/refreezing rate of $-0.10\,m\,a^{-1}$ of ice in the blocky layer. This is comparable to the net-melt rate of $-0.05\,m\,a^{-1}$ found by Kääb et al. (1998) for the same site.

2.6 Simulation of the thermal regime

Figure 5 shows the measured and the simulated temperatures at two depths for the simulated period. The green lines in Fig. 5 show the results for the simulation with only meteorological measurement input and the red lines the results with measured meteorological input as well as an additional seasonal heat source and heat sink in the active layer representing advective and radiative heat fluxes. It can be seen that in the case where no additional heat source or sink is active, thermal conditions do not favour the development of permafrost if local meteorological data is used to drive the model. Temperatures are well above 0 °C in summer down to 11 m below the surface, indicating permafrost is not present in this simulation. In the other case with additional heat source and sink, permafrost is present at the respective depths. The values found by experimental calibration are about 28.9 Wm^{-2} for the heat sink during a period from mid

ESurfD
1, 141–175, 2013

September to mid January. The heat source in the period from June to mid September amounts to 26 Wm^{-2}.

3 Discussion

3.1 Energy balance measurements

Regarding the energy balance measurements there are some general points that need to be adressed. First, the categorization of seasons may be based on prevailing meteorological conditions, processes in the active layer or a combination of both (Westermann et al., 2009; Langer et al., 2011; Schneider et al., 2012). Here, three seasons, approximately based on the heat source and heat sink seasons in the model, were differentiated. This may lead to problems in so far as processes may occur in multiple seasons to different proportions depending on meteorological conditions on the one hand and may counteract each other on the other hand. Thus, an interpretation of typical processes within a season is difficult. Nevertheless, some characteristics in the magnitude and the direction of individual energy balance components are obvious. Also the deviations show seasonal similarities and may even be interpreted as freezing and thawing processes due to their directions. Finally, it also has to be considered that data gaps, systematic measurement errors and parameterizations may have a significant influence on the results presented herein.

In the following, potential sources for discrepancies in the individual energy balance components are discussed in detail.

3.1.1 Net radiation

The factor by which measured incoming radiation is reduced is $\cos 15^{\circ}$, which is assumed to account for both slope and surface geometry. As radiative heat flux at the surface is a very important term in the energy balance small errors in the geometrical correction factor may lead to large uncertainties. A further source of error is a possible

ESurfD
1, 141–175, 2013

underestimation of radiation density during the snow covered season due to a snow cover on the upward looking sensor.

3.1.2 Turbulent fluxes at the surface

Turbulent fluxes, as calculated following Eqs. (4) and (5), are strongly depending on wind speed, which is generally very low at the site. This may partly explain the differences between the magnitude of the sensible heat flux in the measurements and in the model.

3.1.3 Melt energy

The calculation of melt energy based solely on snow height measurements and assuming a constant snow density, as it was done in this study, may lead to errors. Snow density will certainly vary over the winter period in nature reaching a peak in spring with the beginning of snow melt. So, with the assumption of a constant snow density, melt rates will be overestimated in the beginning of winter, when snow is less dense and underestimated in late winter and spring when snow is probably denser than 300 kg m^{-3}. Refreezing of melted snow within the snow cover will lead to more melt than would be expected by measurements of the difference in snow heights. Settlement of snow might be mistaken for melt when occurring above the threshold temperature of −3 °C. During a 24 h period snow melt and snow fall may occur (snow fall in the morning, snow melt in the afternoon) which is not considered in the calculations. This coinciding situation is most likely to occur in the melting period from April to July and in the summer season. Thus the values calculated for the respective period are likely to be too low.

3.1.4 Ground heat flux

The strong influence of the thermal conductivity on the conductive heat flux may lead to significant uncertainties. Further uncertainties are added due to the unknown porosity

ESurfD
1, 141–175, 2013

(fraction of blocks to air filled voids) of the blocky layer, the position of the thermistors in the borehole and the reduction factor chosen in this study.

3.1.5 Net-radiation between adjacent blocks

The calculation of the thermal radiation between adjacent blocks in this study is based on the assumption of three equally large quadratic blocks with an area 1 m^2 parallel stacked with a spacing of 0.33 m. The surface temperatures are assumed to be equal to the temperatures measured at 0.55 m, 1.55 m, 2.55 m, and 3.55 m. This is a rough estimation and may lead to significant uncertainties in the energy balance, especially in seasons with large thermal gradients.

3.1.6 Snow heat flux

Using the temperature at 0.55 m depth instead of the ground surface temperature in Eq. (14) may lead to errors, which can be considered as small due to nearly isothermal conditions in the active layer during the snow covered period.

3.1.7 Energy storage

Errors in the calculation of the energy storage change may be due to assumption of the rock mass, varying rock density and heat capacity as well as borehole temperature measurements.

3.1.8 Turbulent fluxes between blocks

The results of the turbulent heat flux ($Q_{h_{al}}$ and $Q_{le_{al}}$) between the blocks presented here, are based on the work of S. Schneider (personal communication, 2013). Measurements for the calculations were only available for the time period of mid June to mid July 2006, thus values available for the respective period have been taken for the complete summer season of June to September. Values for the other two seasons

ESurfD
1, 141–175, 2013

were not available and are missing in the energy balance. This may produce significant errors in the energy balance in the fall period where these processes have been shown to be large due to the advection of cold air (Panz, 2006).

3.1.9 Deviations

In the model the energy balance is not supposed to be closed due to convective heat transfer by precipitation and snow as well as surface runoff. In the measurements there are other sources of error. Besides the effects of radiative, convective and advective heat transfer, which are subject of this study and are thus expected to cause deviations, there are other sources of error, such as direct measurement errors at the meteorological station, i.e. icing and snow at radiation sensors (see Table 1). Finally, unmeasured freezing and thawing processes within the blocky surface layer can add significant uncertainties to the energy balance.

When summing up all energy balance components following Eq. (1) and considering the energy exchange processes in the blocky layer following Eq. (2) the result is supposed to be zero. As the two terms $Q_{m_{pf}}$ and $Q_{m_{al}}$ in Eq. (2) are unknown, Eq. (1) will have a deviation term to a zero energy balance. This deviation is composed of possible measurement and calculation errors on the one hand and the two missing terms on the other hand. Assuming that the measurement errors will even out, the deviation term could be seen as an indirect measure of the magnitude of unmeasured processes in the blocky surface layer. If it is hypothetesized that the missing processes are mainly associated with freezing and thawing of water in the active layer ($Q_{m_{al}}$) and at the permafrost table ($Q_{m_{pf}}$), then the sum of the deviation terms would be an indirect measure of net-melt or net-refreezing rates. This result can then be compared to the net melt rate found in a study by Kääb et al. (1998) based on geodetic measurements as well as calculations of the vertical deformation of the rock glacier mass over the period from 1987 to 1996. The value −0.05 m per year found by Kääb et al. (1998) is smaller than the one of −0.10 m found in this study. This discrepancy may be due to measurement

ESurfD
1, 141–175, 2013

and parameterization errors on the one hand and/or a real increase in the net-melt rate caused by a warmer climate in recent years on the other.

3.2 Model

The values found for the heat source and sink layer by calibrating the model to match observed borehole temperatures have to be treated with care because the source/sink layer is 1 m thick and placed close to the surface. This means that the heat extracted or added is transferred to larger depths (i.e. the depths shown in Fig. 5) by conduction and percolating water. This transfer will not act immediately on the temperatures at depth but will take some time. In nature however the heat transfer by thermal radiation as well as convection and advection of air in the voids between the blocks may act more directly on the thermal regime in the permafrost below. Because of this phase shift in heat transfer it is possible that the timing of the heat source/sink in the layer, located near the surface, is not identical with the timing of the processes in nature. Furthermore it is not likely that the three-dimensional heat transfer within the blocky layer will be constant over periods of four consecutive months as it is assumed for the parameterization of model. The approach chosen to calibrate a process based permafrost model in this study differs from similar model studies on sites with coarse debris cover (e.g. Gruber and Hoelzle, 2008). The presented solution with a heat source and sink layer is considered to be useful as an additional instrument for both the calibration of the model and for an approximate quantification of three-dimensional heat transfer within the active layer.

3.3 Synopsis

Besides energy balance studies as presented herein, the indirect approach for the quantification of three-dimensional heat transfer by air circulation and longwave radiaton by applying a heat source and sink layer in a permafrost model can serve as an additional instrument in the investigation of such processes. The direct comparison of

ESurfD
1, 141–175, 2013

model parameters for the heat sink and source with the deviations found in energy balance measurements is difficult to interpret because of possible measurement errors on the one hand and process simplification in the model on the other. The comparison of the measured and the simulated energy balance reveals large differences for some of the components, especially the sensible heat flux during the summer season. This can be attributed to the different reference units (unit area versus volumetric surface layer) in the model and the measurements and to a correction parameter in the Coup Model, which enhances turbulent exchange during periods with low wind speeds. Measured energy fluxes are studied in a volumetric surface layer which includes processes such as radiative heat transfer between blocks in the nature. As such processes are not integrated in the model, they are likely to be compensated by other heat transfer mechanisms. A surplus of energy at the surface in the model will not completely be transferred to the ground but rather be emitted to the atmosphere by turbulent fluxes and longwave radiation. This difference will be most significant in the summer season, as typically measured wind speeds tend to be low during this period. In the model turbulent fluxes are enhanced by a correction parameter during such conditions.

4 Conclusions

In this study we applied a numerical permafrost model integrating freezing and thawing processes and a dynamical snow cover to simulate a 13 yr period of the active layer and the permafrost at rock glacier Murtèl-Corvatsch in the Upper Engadine, Swiss Alps. Other than considering the blocky layer with voids as a thermal semi-conductor, a different approach is presented, which integrates a heat source and sink in the active layer. A measured energy balance over a volumetric surface layer including terms for radiative heat transfer between adjacent blocks, turbulent fluxes in the active layer and energy storage change is presented and compared to the modeled energy balance at the site. The deviations in the measured energy balance were used to indirectly

ESurfD
1, 141–175, 2013

quantify unmeasured latent heat processes involving freezing and thawing processes in the active layer and at the permafrost table.

- The approach chosen to calibrate a process-based permafrost model differs from similar model studies on sites with coarse debris cover. The presented solution with a heat source and sink layer is considered to be useful for both the calibration of the model and the approximate quantification of three-dimenstional heat transfer processes within the active layer, which so far can not be modelled explicitly.
- The unmeasured heat transfer processes within the blocky active layer could be approximated in the model to act as a heat sink of 28.9 Wm^{-2} during a period form mid September to mid January and as a heat source in the period from June to mid September of 26 Wm^{-2}.
- Measured and simulated energy balances differ significantly. The differences can partly be attributed to the different reference units (i.e. a unit area in the model and a volumetric surface layer in the measurements) and thus different energy exchange processes.
- The integration of additional energy balance components reduced the deviations to a zero energy balance significantly compared to earlier studies at the same site (Mittaz et al., 2002).
- The remaining deviations in the measured energy balance are hypothesized to be due to latent heat effects (i.e. freezing and thawing) in the active layer and at the permafrost table. This hypothesis is supported by the results of an earlier study by Kääb et al. (1998), which showed a net melt rate of the same order of magnitude at the same site.

In future studies the emphasis should be on both, more detailed measurements of energy balance components including the blocky layer (i.e. heat transfer by longwave radiation and turbulent fluxes due to convective and advective air circulation), and a

ESurfD
1, 141–175, 2013

more physically based modeling of the heat source and sink terms, i.e. the representation of radiation coupled with thermal gradients in the active layer and air flow coupled to meteorological conditions.

Acknowledgements. This study was part of the german Bündelproject "Sensitivity of mountain Permafrost to Climate Change" (SPCC, http://www.spcc-project.de/ funded by the German national Science Foundation (DFG, HA3475/3-1)) and the Swiss National Science Foundation project "The evolution of mountain permafrost in Switzerland" (TEMPS, SNF, CRSII2_136279). We would like to thank the Swiss Permafrost Monitoring Network (PERMOS) for providing the measurement data. We also thank the Corvatsch Bergbahn AG for transport and accommodation.

References

Arenson, L., Hoelzle, M., and Springman, S.: Borehole deformation measurements and internal structure of some rock glaciers in Switzerland, Permafrost Periglac., 13, 117–135, doi:10.1002/ppp.414, 2002. 143, 145

Arenson, L., Hauck, C., Hilbich, C., Seward, L., Yamamoto, Y., and Springman, S.: Sub-surface heterogeneities in the Murtèl-Corvatsch rock glacier, Switzerland, in: Proceedings of the 6th Canadian Permafrost Conference, 1494–1500, 2010. 145

Balch, E. S.: Glaciers or freezing caverns, Allen, Lane and Scott, Philadelphia, PA, 1900. 143

Bayard, D., Staehli, M., Parriaux, A., and Fluehler, H.: The influence of seasonally frozen soil on the snowmelt runoff at two alpine sites in southern Switzerland, J. Hydrol., 309, 66–84, doi:10.1016/j.jhydrol.2004.11.012, 2005. 153

Binxiang, S., Lijun, Y., and Xuezu, X.: Onset and evaluation on winter-time natural convection cooling effectiveness of crushed-rock highway embankment, Cold Reg. Sci. Technol., 48, 218–231, 2007. 144

Cheng, G. D., Lai, Y. M., San, Z. Z., and Jiang, F.: The "thermal semi-conductor" effect of crushed rocks, Permafrost Periglac., 18, 151–160, 2007. 144

Delaloye, R. and Lambiel, C.: Evidence of winter ascending air circulation throughout talus slopes and rock glaciers situated in the lower belt of alpine discontinuous permafrost (Swiss Alps), Norsk Geogr. Tidssk., 59, 194–203, doi:10.1080/00291950510020673, 2005. 143, 153

ESurfD

1, 141–175, 2013

Delaloye, R., Reynard, E., Lambiel, C., Marescot, L., and Monnet, R.: Thermal anomaly in a cold scree slope (Creux du Van, Switzerland), in: Proceedings of the 8th International Conference on Permafrost, Zurich, Switzerland, edited by: Phillips, M., Springman, S. M., and Arenson, L., 175–180, Balkema Publishers, Lisse, 2003. 144

Devaux, J.: Radiothermic economy of fields of snow and glaciers, Science Abstr., Serias A, 36, 980–981, 1933. 152

Fillion, M.-H., Côté, J., and Konrad, J.-M.: Thermal radiation and conduction properties of materials ranging from sand to rock-fill, Can. Geotech. J., 48, 532–542, 2011. 145

Gruber, S. and Hoelzle, M.: The cooling effect of coarse blocks revisited: a modeling study of a purely conductive mechanism, in: 9th Int. Conf. on Permafrost, Institute of Northern Engineering, Fairbanks, University of Alaska, 29 June–3 July 2008, edited by: Kane, D. and Hinkel, K., 557–561, 2008. 144, 160

Gustafsson, D., Stähli, M., and Jansson, P.-E.: The surface energy balance of a snow cover: comparing measurements to two differentsimulation models, Theor. Appl. Climatol., 70, 81–96, 2001. 153

Haeberli, W., Huder, J., Keusen, H., Pika, J., and Röthlisberger, H.: Core drilling through rock glacier-permafrost, in: Proceedings of the Fifth International Conference on Permafrost, Vol. 2, 937–942, by Senneset-Kaare, 1988. 146

Hanson, S. and Hoelzle, M.: The thermal regime of the active layer at the Murtèl rock glacier based on data from 2002, Permafrost Periglac., 15, 273–282, doi:10.1002/ppp.499, 2004. 143, 153

Harris, S. A. and Pedersen, D. E.: Thermal regimes beneath coarse blocky materials, Permafrost Periglac., 9, 107–120, doi:10.1002/(SICI)1099-1530(199804/06)9:2<107::AID-PPP277>3.0.CO;2-G, 1998. 143, 144

Herz, T., King, L., and Gubler, H.: Microclimate within coarse debris of talus slopes in the alpine periglacial belt and its effect on permafrost, in: Proceedings of the 8th International Conference on Permafrost, Zurich, Switzerland, edited by: Phillips, M., Springman, S. M., and Arenson, L., 383–387, Balkema Publishers, Lisse, 2003. 143

Hoelzle, M. and Gruber, S.: Borehole and ground surface temperatures and their relationship to meteorological conditions in the Swiss Alps, in: 9th Int. Conf. on Permafrost, Institute of Northern Engineering, Fairbanks, University of Alaska, 29 June–3 July 2008, edited by: Kane, D. L. and Hinkel, K. M., 723–728, 2008. 145, 146

ESurfD

1, 141–175, 2013

Hoelzle, M., Vonder Mühll, D., and Haeberli, W.: Thirty years of permafrost research in the Corvatsch - Furtschellas area, Eastern Swiss Alps: A review, Norsk Geogr. Tidsskr., 56, 137–145, doi:10.1080/00291950276005646 8, 2002. 145, 146

Jansson, P.-E. and Karlberg, L.: Coupled heat and mass transfer model for soil-plant-atmosphere systems, Royal Institute of Technology, Dept of Civil and Environmental Engineering, Stockholm, http://www.lwr.kth.se/Vara%20Datorprogram/CoupModel/index.htm, 2011. 153

Johnsson, H. and Lundin, L.-C.: Surface runoff and soil water percolation as affected by snow and soil frost, J. Hydrol., 122, 141–159, doi:10.1016/0022-1694(91)90177-J, 1991. 153

Kääb, A., Gudmundsson, G. H., and Hoelzle, M.: Surface deformation of creeping mountain permafrost. Photogrammetric investigations on rock glacier Murtèl, Swiss Alps, in: Proceedings of the 7th International Conference on Permafrost, 531–537, 1998. 143, 155, 159, 162

Keller, F. U.: Interaktionen zwischen Schnee und Permafrost: Eine Grundlagenstudie im Oberengadin, Ph.D. thesis, Dissertation an der Abteilung Naturwissenschaften der Eidgenössisch Technischen Hochschule Zürich, 1994. 152

Kunii, D. and Smith, J.: Heat transfer characteristics of porous rocks, AIChE J., 6, 71–78, 1960. 145, 151

Langer, M., Westermann, S., Muster, S., Piel, K., and Boike, J.: The surface energy balance of a polygonal tundra site in northern Siberia – Part 2: Winter, The Cryosphere, 5, 509–524, doi:10.5194/tc-5-509-2011, 2011. 156

Lundin, L. C.: Hydraulic properties in an operational model of frozen soil, J. Hydrol., 118, 289–310, doi:10.1016/0022-1694(90)90264-X, 1990. 153

McAdams, W. H.: Heat transmission, McGraw-Hill Book Co., Inc., New York, NY, 1954. 151

Mittaz, C., Hoelzle, M., and Haeberli, W.: First results and interpretation of energy-flux measurements over Alpine permafrost, Ann. Glaciol., 31, 275–280, doi:10.3189/172756400781820363, 2000. 143, 145, 146, 153, 154

Mittaz, C., Imhof, M., Hoelzle, M., and Haeberli, W.: Snowmelt Evolution Mapping Using an Energy Balance Approach over an Alpine Terrain, Arct. Antarct. Alp. Res., 34, 274–281, 2002. 162

Oke, T. R.: Boundary layer climates, Routledge, 1988. 147, 148

Panz, M.: Analyse von Austauschprozessen in der Auftauschicht des Blockgletschers Murtèl-Corvatsch, Oberengadin, Master's thesis, Ruhr Universität (unpublished), 2006. 159

ESurfD

1, 141–175, 2013

Scherler, M., Hauck, C., Hoelzle, M., Stähli, M., and Völksch, I.: Meltwater infiltration into the frozen active layer at an alpine permafrost site, Permafrost Periglac., 21, 325–334, doi:10.1002/ppp.694, 2010. 153

Scherler, M., Hauck, C., Hoelzle, M., and Salzmann, N.: Modeled sensitivity of two alpine permafrost sites to RCM-based climate scenarios, J. Geophys. Res., doi:10.1002/jgrf.20069, in press, 2013. 144, 153

Schneider, S., Hoelzle, M., and Hauck, C.: Influence of surface and subsurface heterogeneity on observed borehole temperatures at a mountain permafrost site in the Upper Engadine, Swiss Alps, The Cryosphere, 6, 517–531, doi:10.5194/tc-6-517-2012, 2012. 145, 146, 156

Stähli, M., Jansson, P.-E., and Lundin, L.-C.: Preferential water flow in a frozen soil – a two-domain model approach, Hydrol. Process., 10, 1305–1316, doi:10.1002/(SICI)1099-1085(199610)10:10<1305::AID-HYP462>3.0.CO;2-F, 1996. 153

Stocker-Mittaz, C.: Permafrost distribution modeling based on energy balance data, Ph.D. thesis, Univ. of Zurich, Zurich, Switzerland, 2002. 147, 152

Tanaka, H., Nohara, D., and Yokoi, M.: Numerical simulation of wind hole circulation and summertime ice formation at Ice Valley in Korea and Nakayama in Fukushima, Japan, Journal-Meteorological Society of Japan, Series 2, 78, 611–630, 2000. 144

Vonder Mühll, D., Arenson, L., and Springman, S.: Two new boreholes through the Murtèl–Corvatsch rock glacier, Upper Engadin, Switzerland, in: 1st European Permafrost Conference, Abstract, p. 83, 2001. 145

Vonder Mühll, D., Arenson, L., and Springman, S.: Temperature conditions in two Alpine rock glaciers, in: 8th International Conference on Permafrost, Zürich, Swets & Zeitlinger, Lisse, 1195–1200, 2003. 144, 146

Wakonigg, H.: Unterkühlte schutthalden, Arbeiten aus dem Institut für Geographie der Karl-Franzens-Universität Graz, 33, 209–223, 1996. 143

Westermann, S., Lüers, J., Langer, M., Piel, K., and Boike, J.: The annual surface energy budget of a high-arctic permafrost site on Svalbard, Norway, The Cryosphere, 3, 245–263, doi:10.5194/tc-3-245-2009, 2009. 143, 147, 156

Williams, P. J. and Smith, M. W.: The frozen earth: fundamentals of geocryology, Vol. 306, Cambridge University Press Cambridge, 1989. 147

ESurfD

1, 141–175, 2013

Table 1. Meteorological station equipment and accuracy.

Variable	Sensor	Sensor Type	Accuracy
	Logger (Campbell)	Data logger CR10X; interval timer SDM-INT8; multiplexer AM416	
Radiation (short- and longwave)	Netradiometer CNR1 (Kipp & Zonen)	2 pyranometer CM3; 2 pyrgeometer CG3; Pt-100 temp. sensor	±10 %; ±2 K
Air Temperature/ Humidity	Hygrometer MP-100A ventilated (Rotronic)	RTD Pt-100; Hygrometers C94	±10 %
Wind Speed	Model 05103-5 (Young)	Potentiometer	±0.3 m s^{-1}
Snow Height	SR50 (Campbell)	Ultrasonic Electrostatic Transducer	±0.01 m
Surface Temperature	Infrared thermometer	Irt/c.5	±1.5 °C
Borehole Temperatures	YSI 44006 (Yellow Springs Instruments)	NTC-Thermistors	±0.02 °C
Precipitation	MeteoSwiss (Corvatsch summit)	Rain gauge	±30 %

ESurfD
1, 141–175, 2013

Table 2. Seasonal (June–September) averages of the energy balance components with deviations (in Wm^{-2}) and correponding ice thickness equivalents (in m). Years marked with a star were not considered for the calculation of the average and the standard deviation.

Year	Q_r	Q_h	Q_{le}	Q_m	Q_s	$Q_{g_{al}}$	$Q_{r_{al}}$	Q_{st}	Q_t	Q_{pf}	dev	ice
1997*	80.0	−15.2	−22.2	–	–	−21.0	−6.9	−1.5	−0.5	−1.1	−11.6	−0.40
1998*	–	−11.7	−12.5	−15.0	0.0	−24.1	−7.9	−0.3	−0.5	−1.2	73.2	2.52
1999*	69.1	−14.1	−22.6	−5.5	0.0	−25.7	−8.5	−2.3	−0.5	−1.6	11.7	0.40
2000*	89.7	−13.8	−20.8	−11.6	0.0	−21.4	−7.1	0.0	−0.5	−1.3	−13.0	−0.45
2001*	81.1	−7.9	−16.0	−21.8	0.2	−2.9	−1.0	4.5	−0.5	−0.6	−35.2	−1.21
2002	75.1	−11.2	−19.5	−8.7	0.1	−24.9	−8.2	−0.8	−0.5	−1.8	0.3	0.01
2003*	85.4	−11.3	−20.5	−2.7	0.0	−33.9	−11.2	−0.3	−0.5	−1.0	−4.1	−0.14
2004	81.3	−11.0	−18.8	−8.6	0.0	−27.9	−9.2	−1.3	−0.5	−1.3	−2.6	−0.09
2005	88.4	−17.7	−25.8	–	–	−25.2	−8.3	−0.3	−0.5	−1.7	−9.1	−0.31
2006	89.3	−14.3	−24.3	−3.3	–	−28.3	−9.3	−1.4	−0.5	−1.8	−6.2	−0.21
2007	91.9	−17.6	−26.5	−2.8	0.0	−24.6	−8.1	−0.1	−0.5	−1.1	−10.6	−0.37
Average	85.3	−13.1	−21.5	−8.5	0.1	−23.6	−7.8	0.0	−0.5	−1.3	−5.6	−0.19
Stdev	6.9	2.8	4.0	6.0	0.1	7.4	2.4	1.7	–	0.3	4.0	0.14

ESurfD
1, 141–175, 2013

Table 3. Seasonal (October–January) averages of the energy balance components with deviations (in Wm^{-2}) and correponding ice thickness equivalents (in m). Years marked with a star were not considered for the calculation of the average and the standard deviation.

Year	Q_r	Q_h	Q_{le}	Q_m	Q_s	$Q_{g(al)}$	$Q_{r(al)}$	Q_{st}	Q_t	Q_{pf}	dev	ice
1997*	−31.1	6.6	0.6	−1.3	−1.6	−5.5	−1.9	3.8	–	−0.6	31.0	1.05
1998*	−41.4	26.8	7.6	−17.7	−4.2	6.2	2.2	1.7	–	−0.1	18.7	0.63
1999*	−33.0	18.9	4.4	−4.1	−2.2	2.5	1.1	2.1	–	−0.4	10.7	0.36
2000*	−22.1	19.2	6.1	−15.2	−1.5	2.3	1.1	1.1	–	−0.6	9.5	0.32
2001*	−37.5	14.1	3.4	−4.3	0.0	14.8	5.0	2.8	–	0.7	1.0	0.03
2002	−19.3	14.0	4.1	−18.2	−0.8	2.2	1.1	0.9	–	−0.9	16.9	0.57
2003*	−28.7	25.0	6.7	−14.1	−2.7	6.8	2.6	2.2	–	−0.1	2.3	0.08
2004	−37.2	23.5	5.4	−14.3	−1.6	9.0	3.2	3.0	–	0.1	9.0	0.30
2005	−36.8	13.3	3.3	−0.3	–	13.0	5.0	3.1	–	0.1	−0.8	−0.03
2006	−30.1	16.7	5.2	−13.6	−1.8	7.1	2.8	2.9	–	−0.5	11.3	0.38
2007	−31.2	18.8	4.8	−6.6	−1.6	10.8	4.0	2.4	–	0.2	−1.5	−0.05
Average	−31.7	17.9	4.7	−10.0	−1.8	6.7	2.4	2.4	–	−0.2	6.8	0.24
Stdev	6.4	5.6	1.8	6.4	1.0	5.5	1.9	0.8	–	0.5	6.4	0.24

ESurfD
1, 141–175, 2013

Table 4. Seasonal (February–May) averages of the energy balance components with deviations (in Wm^{-2}) and correponding ice thickness equivalents (in m). Years marked with a star were not considered for the calculation of the average and the standard deviation.

Year	Q_r	Q_h	Q_{le}	Q_m	Q_s	$Q_{g(al)}$	$Q_{r(al)}$	Q_{st}	Q_t	Q_{pf}	dev	ice
1997*	−10.8	−1.2	−1.5	–	–	−0.7	−1.7	–	–	0.1	15.9	0.55
1998*	−38.7	8.8	2.0	−14.9	−1.8	0.6	1.0	−1.0	–	0.2	44.0	1.51
1999*	1.9	16.5	6.0	−26.4	−2.3	0.5	1.0	−1.8	–	0.5	4.0	0.14
2000*	−3.3	16.7	5.4	−10.7	−2.1	0.6	0.8	−0.4	–	−0.1	−6.9	−0.24
2001*	30.0	18.7	6.6	−20.7	−1.2	1.5	2.0	0.6	–	0.3	−37.7	−1.30
2002	−1.9	14.3	4.9	−14.7	−2.4	−0.4	0.5	−2.3	–	0.9	1.2	0.04
2003*	−7.4	10.2	7.7	−18.1	−1.1	1.1	1.3	−2.1	–	0.0	8.4	0.29
2004	1.6	18.6	4.7	−11.0	−2.1	0.8	1.5	−1.2	–	0.5	−13.3	−0.46
2005	9.6	16.2	4.2	−24.7	−2.9	0.6	1.4	−2.6	–	0.6	−2.4	−0.08
2006	5.9	9.5	3.0	−16.4	–	0.9	1.6	−2.6	–	0.4	−2.2	−0.07
2007	18.2	13.4	1.8	−16.7	−2.2	−0.7	−0.2	−2.0	–	−0.3	−11.3	−0.39
Average	6.6	14.7	4.8	−15.5	−2.0	0.6	1.1	−1.6	–	0.3	−2.2	−0.14
Stdev	16.6	5.6	2.5	5.0	0.5	0.7	1.0	1.0	–	0.3	7.2	0.19

ESurfD
1, 141–175, 2013

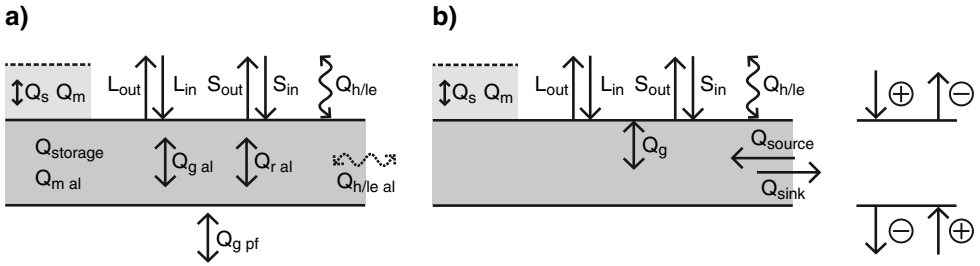

Fig. 1. Illustration of the different energy exchange processes in **(a)** the energy balance calculations and **(b)** in the Coup Model. The scheme on the right hand side shows the convention of positive and negative fluxes.

ESurfD
1, 141–175, 2013

Heat transfer processes in the active layer of rock glacier Murtèl

M. Scherler et al.

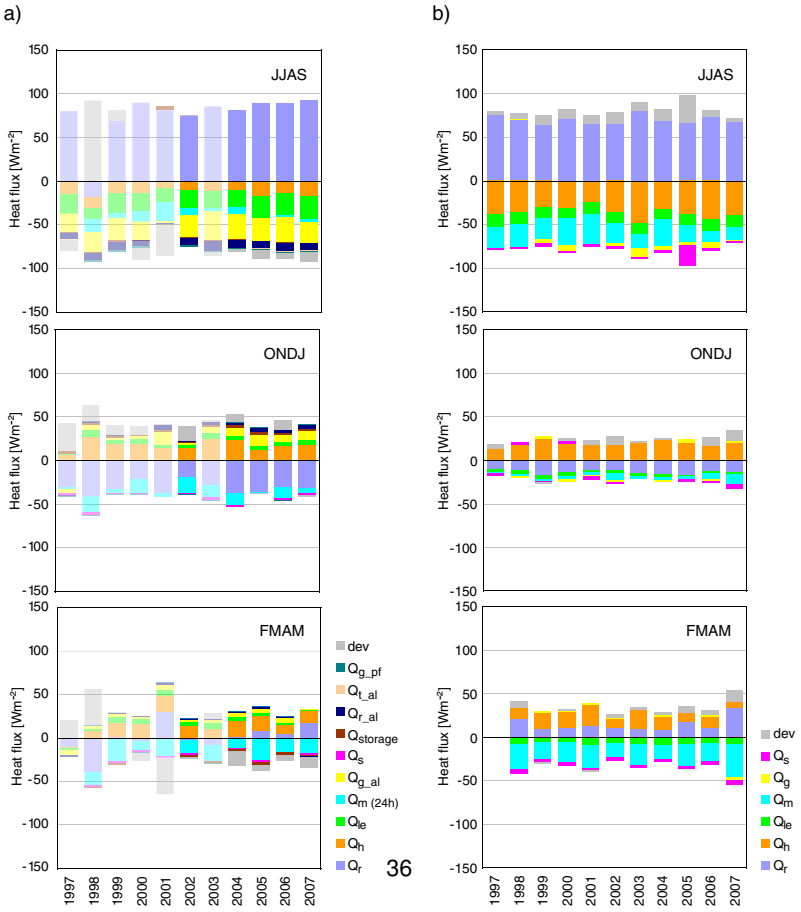

Fig. 2. Seasonal energy balance components at rock glacier Murtèl-Corvatsch. **(a)** shows the observations and **(b)** shows the modeled components.

ESurfD
1, 141–175, 2013

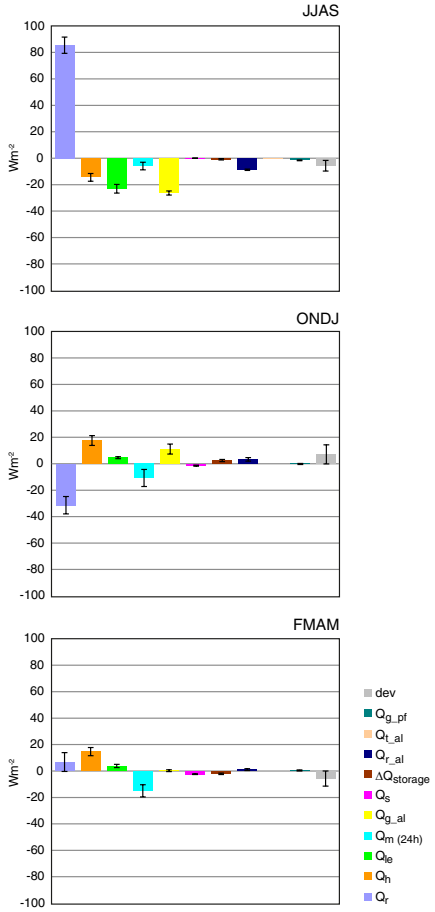

Fig. 3. 5 yr averages (with corresponding standard deviations) of the seasonal energy balance components at rock glacier Murtèl-Corvatsch.

ESurfD
1, 141–175, 2013

Heat transfer processes in the active layer of rock glacier Murtèl

M. Scherler et al.

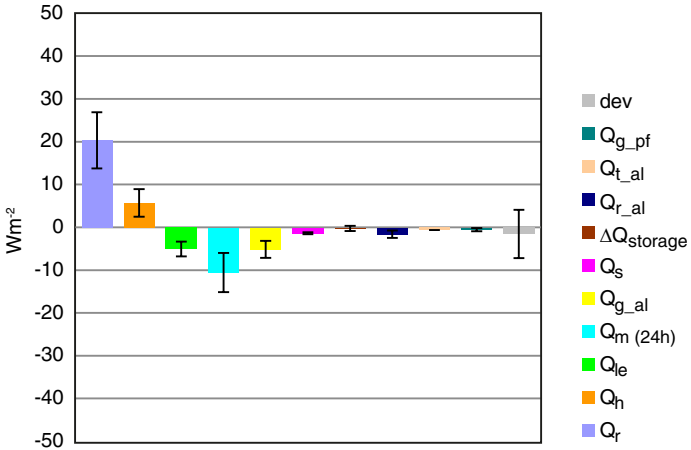

Fig. 4. 5 yr averages over all three seasons (with corresponding standard deviations) of the energy balance components at rock glacier Murtèl-Corvatsch.

ESurfD
1, 141–175, 2013

Heat transfer processes in the active layer of rock glacier Murtèl

M. Scherler et al.

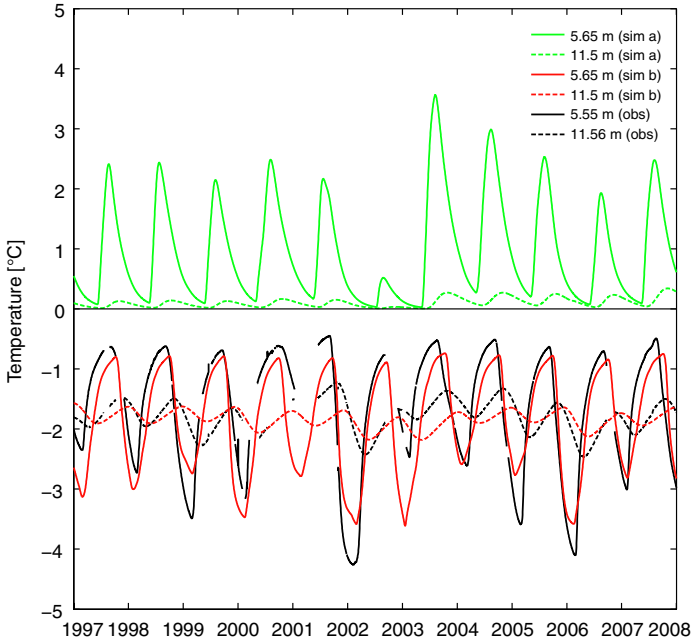

Fig. 5. Temperature results of the calibration phase of the Coup Model at rock glacier Murtèl-Corvatsch.

ESurfD
1, 141–175, 2013

Heat transfer processes in the active layer of rock glacier Murtèl

M. Scherler et al.